

Quantum Hall Effect in a Gate-Controlled p - n Junction in Graphene

J. R. Williams,¹ L. DiCarlo,² and C. M. Marcus²

¹*School of Engineering and Applied Science, Harvard University, Cambridge, MA 02138, USA*

²*Department of Physics, Harvard University, Cambridge, MA 02138, USA*

(Dated: February 11, 2013)

The unique band structure of graphene allows reconfigurable electric-field control of carrier type and density, making graphene an ideal candidate for bipolar nanoelectronics. We report on the realization of a single-layer graphene p - n junction in which carrier type and density in two adjacent regions are locally controlled by electrostatic gating. Transport measurements in the quantum Hall regime reveal new plateaus of two-terminal conductance across the junction at 1 and $3/2$ times the quantum of conductance, e^2/h , consistent with recent theory. Beyond enabling investigations in condensed matter physics, the local-gating technique demonstrated here sets the foundation for a future graphene-based bipolar technology.

Graphene, a single-layer hexagonal lattice of carbon atoms, has recently emerged as a fascinating system for fundamental studies in condensed matter physics [1], as well as a candidate for novel sensors [2, 3] and post-silicon electronics [4, 5, 6, 7, 8, 9, 10]. The unusual band structure of single-layer graphene makes it a zero-gap semiconductor with a linear (photon-like) energy-momentum relation near the points where valence and conduction bands meet. Carrier type—electron-like or hole-like—and density can be controlled using the electric-field effect [10], obviating conventional semiconductor doping, for instance via ion implantation. This feature, doping via local gates, would allow graphene-based bipolar technology—devices comprising junctions between hole-like and electron-like regions, or p - n junctions—to be reconfigurable, using only gate voltages to distinguish p (hole-like) and n (electron-like) regions within a single sheet. While global control of carrier type and density in graphene using a single back gate has been investigated by several groups [11, 12, 13], local control [8, 9] of single-layer graphene has remained an important technological milestone. In addition, p - n junctions are of great interest for low-dimensional condensed matter physics. For instance, recent theory predicts that a local step in potential would allow solid-state realizations of relativistic (“Klein”) tunneling [14, 15], and a surprising scattering effect known as Veselago lensing [16], comparable to scattering of electromagnetic waves in negative-index materials [17].

We report on the realization of local top gating in a single-layer graphene device which, combined with global back gating, allows individual control of carrier type and density in adjacent regions of a single atomic layer. Transport measurements at zero perpendicular magnetic field B and in the quantum Hall (QH) regime demonstrate that the functionalized aluminum oxide (Al_2O_3) separating the graphene from the top gate does not significantly dope the layer nor affect its low-frequency transport properties. We study the QH signature of the graphene p - n junction, finding new conductance plateaus at 1 and $3/2$ e^2/h , consistent with recent theory address-

ing equilibration of edge states at the p - n interface [18].

Graphene sheets are prepared via mechanical exfoliation using a method similar to that used in Ref. 10. Graphite flakes are deposited on 300 nm of SiO_2 on a degenerately doped Si substrate. Inspection with an optical microscope allows potential single-layer regions of graphene to be identified by a characteristic coloration that arises from thin-film interference. These micron-scale regions are contacted with thermally evaporated Ti/Au (5/40 nm), and patterned using electron-beam lithography. Next, a ~ 30 nm layer of oxide is deposited atop the entire substrate. As illustrated (Fig. 1B), the oxide consists of two parts: a non-covalent functionaliza-

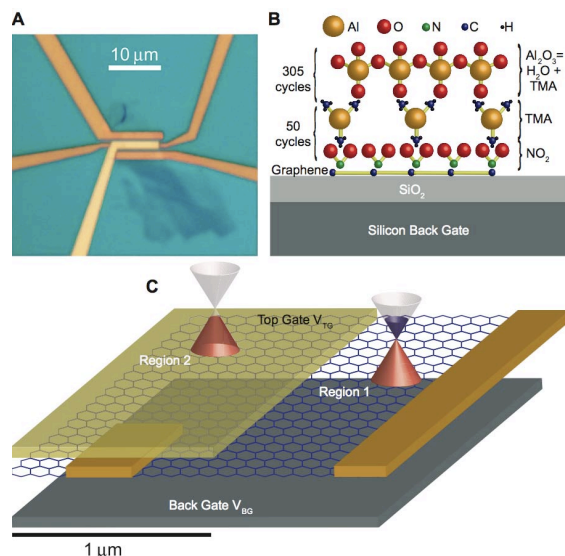


FIG. 1: (A) Optical micrograph of a device similar to the one measured. Metallic contacts and top gate appear in orange and yellow, respectively. Darker regions below the contacts are thicker graphite from which the contacted single layer of graphene extends. (B) Illustration of the oxide deposition process. A non-covalent functionalization layer is first deposited using NO_2 and TMA (50 cycles) and Al_2O_3 is then grown by atomic layer deposition using H_2O -TMA (305 cycles yielding ~ 30 nm thickness). (C) Schematic diagram of the device measured in this experiment.

tion layer (NCFL) and Al_2O_3 . This deposition technique is based on a recipe successfully applied to carbon nanotubes [19]. The NCFL serves two purposes. One is to create a non-interacting layer between the graphene and the Al_2O_3 and the other is to obtain a layer that is catalytically suitable for the formation of Al_2O_3 by atomic layer deposition (ALD). The NCFL is synthesized by 50 pulsed cycles of NO_2 and trimethylaluminum (TMA) at room temperature inside an ALD reactor. Next, 5 cycles of H_2O -TMA are applied at room temperature to prevent desorption of the NCFL. Finally, Al_2O_3 is grown at 225°C with 300 H_2O -TMA ALD cycles. To complete the device, a second step of electron-beam lithography defines a local top gate (5/40 nm Ti/Au) covering a region of the device that includes one of the metallic contacts.

A completed device, similar in design to that shown in the optical image in Fig. 1A, was cooled in a ^3He refrigerator and characterized at temperatures T of 250 mK and 4.2 K. Differential resistance $R = dV/dI$, where I is the current and V the source-drain voltage, was measured by standard lock-in techniques with a current bias of 1 (10) nA_{rms} at 95 Hz for $T = 250$ mK (4.2 K). The voltage across two contacts on the device, one outside the top-gate region and one underneath the top gate, was measured in a four-wire configuration, eliminating series resistance of the cryostat lines. A schematic of the device is shown in Fig. 1C.

The differential resistance R as a function of back-gate voltage V_{BG} and top-gate voltage V_{TG} at $B = 0$ (Fig. 2A), demonstrates independent control of carrier type and density in the two regions. This two-dimensional (2D) plot reveals a skewed, cross-like pattern that separates the space of top-gate and back-gate voltages into four quadrants of well-defined carrier type in the two regions of the sample. The horizontal (diagonal) ridge corresponds to charge neutrality, i.e., the Dirac point, in region 1 (2). The slope of the charge-neutral line in region 2, along with the known distances to the top gate and back gate, gives a dielectric constant $\kappa \sim 6$ for the functionalized Al_2O_3 . The center of the cross at $(V_{TG}, V_{BG}) \sim (-0.2 \text{ V}, -2.5 \text{ V})$ corresponds to charge neutrality across the entire graphene sample. Its proximity to the origin of gate voltages demonstrates that the functionalized oxide does not chemically dope the graphene significantly.

Slices through the 2D conductance plot at fixed V_{TG} are shown in Fig. 2C. The slice at $V_{TG} = 0$ shows a single peak commonly observed in devices with only a global back gate [10, 11, 12, 13]. Using a Drude model away from the charge-neutrality region, mobility is estimated at $\sim 7000 \text{ cm}^2/\text{Vs}$ [10]. The peak width, height, and back-gate position are consistent with single-layer graphene [11, 12, 13] and provides evidence that the electronic structure and degree of disorder of the graphene is not strongly affected by the oxide. Slices at finite $|V_{TG}|$ reveal a doubly-peaked structure. The weaker

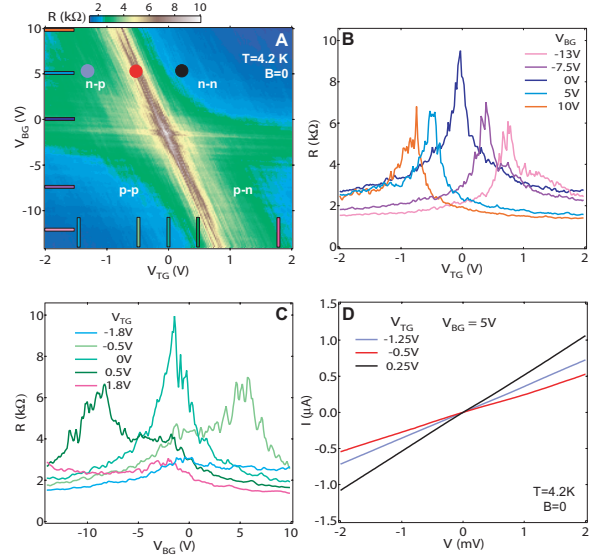


FIG. 2: (A) Two-terminal differential resistance R as a function of the top-gate voltage V_{TG} and back-gate voltage V_{BG} at $B = 0$ and $T = 4.2$ K, demonstrating independent control of carrier type and density in regions 1 and 2. Labels in each of the four quadrants indicate the carrier type (first letter indicates carrier type in region 1). (B and C) Horizontal (Vertical) slices at V_{BG} (V_{TG}) settings corresponding to the colored lines superimposed on Fig. 2A. (D) I - V curves at the gate voltage settings corresponding to the solid circles in Fig. 2A are representative of the linear characteristics observed everywhere in the plane of gate voltages.

peak, which remains near $V_{BG} \sim -2.5 \text{ V}$ at all V_{TG} , corresponds to the Dirac point of region 1. The stronger peak, which moves linearly with V_{TG} , is the Dirac point for region 2. The difference in peak heights is a consequence of the different aspect ratios of regions 1 and 2. Horizontal slices at fixed V_{BG} corresponding to the horizontal lines in Fig. 2A are shown in Fig. 2B. These slices show a single peak corresponding to the Dirac point of region 2. This peak becomes asymmetric away from the charge-neutrality point in region 1. We note that the V_{BG} dependence of the asymmetry is opposite to that observed in Ref. 9, where the asymmetry is studied in greater detail. The changing background resistance results from the different density in region 1 at each V_{BG} setting. Current-voltage (I - V) characteristics, measured throughout the (V_{TG}, V_{BG}) plane, show no sign of rectification in any of the four quadrants or at either of the charge-neutral boundaries between quadrants (Fig. 2D), as expected for reflectionless (“Klein”) tunneling at the p - n interface [14, 15].

In the QH regime at large B , the Dirac-like energy spectrum of graphene gives rise to a characteristic series of QH plateaus in conductance, reflecting the presence of a zero-energy Landau level, that includes only odd multiples of $2e^2/h$ (that is, $2, 6, 10, \dots \times e^2/h$) for uniform carrier density in the sheet [20, 21, 22]. These plateaus can be understood in terms of an odd number of QH edge states (including a zero-energy edge state) at the edge of

the sheet, circulating in a direction determined by the direction of B and the carrier type. The situation is somewhat more complicated when varying local density and carrier type across the sample.

A 2D color plot of differential conductance $g = 1/R$ as a function of V_{BG} and V_{TG} at $B = 4$ T is shown in Fig. 3A. A vertical slice at $V_{TG} = 0$ through the p - p and n - n quadrants (Fig. 3B) reveals conductance plateaus at 2 , 6 , and 10 e^2/h in both quadrants, demonstrating that the sample is single-layer and that the oxide does not significantly distort the Dirac spectrum.

QH features are investigated for differing filling factors ν_1 and ν_2 in regions 1 and 2 of the graphene sheet. A horizontal slice through Fig. 3A at filling factor $\nu_1 = 6$ is shown in Fig. 3C. Starting from the n - n quadrant, plateaus are observed at 6 e^2/h and 2 e^2/h at top-gate voltages corresponding to filling factors $\nu_2 = 6$ and 2 , respectively. Crossing over to the n - p quadrant by further decreasing V_{TG} , a new plateau at $3/2$ e^2/h appears for $\nu_2 = -2$. In the $\nu_2 = -6$ region, no clear QH plateau is observed. Another horizontal slice at $\nu_1 = 2$ shows 2 e^2/h plateaus at both $\nu_2 = 6$ and 2 (see Fig. 3D). Crossing into the n - p quadrant, the conductance exhibits QH plateaus at 1 e^2/h for $\nu_2 = -2$ and near $3/2$ e^2/h for $\nu_2 = -6$.

For ν_1 and ν_2 of the same sign (n - n or p - p), the observed conductance plateaus follow

$$g = \min(|\nu_1|, |\nu_2|) \times e^2/h. \quad (1)$$

This relation suggests that the edge states common to both regions propagate from source to drain while the remaining $|\nu_1 - \nu_2|$ edge states in the region of highest absolute filling factor circulate internally within that region and do not contribute to the conductance. This picture is consistent with known results on conventional 2D electron gas systems with inhomogeneous electron density [23, 24, 25].

Recent theory [18] addresses QH transport for filling factors with opposite sign in regions 1 and 2 (n - p and p - n). In this case, counter-circulating edge states in the two regions travel in the same direction along the p - n interface (Fig. 3F), which presumably facilitates mode mixing between parallel-traveling edge states. For the case of complete mode-mixing—that is, when current entering the junction region becomes uniformly distributed among the $|\nu_1| + |\nu_2|$ parallel-traveling modes—quantized plateaus are expected [18] at values

$$g = \frac{|\nu_1||\nu_2|}{|\nu_1| + |\nu_2|} \times e^2/h. \quad (2)$$

A table of the conductance plateau values given by Eqs. 1 and 2 is shown in Fig. 3E. Plateau values at 1 e^2/h for $\nu_1 = -\nu_2 = 2$ and at $3/2$ e^2/h for $\nu_1 = 6$ and $\nu_2 = -2$ are observed in experiment. Notably, the $3/2$ e^2/h plateau suggests uniform mixing among four edge stages

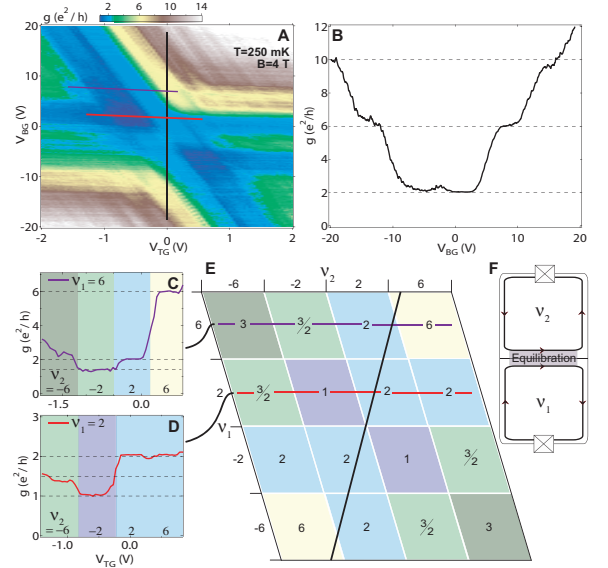


FIG. 3: (A) Differential conductance g as a function of V_{TG} and V_{BG} at $B = 4$ T and $T = 250$ mK. (B) Vertical slice at $V_{TG} = 0$, traversing p - p and n - n quadrants. Plateaus are observed at 2 e^2/h and 6 e^2/h , the quantum Hall signature of single-layer graphene. (C) Horizontal slice at $\nu_1 = 6$ showing conductance plateaus at 6 , 2 and $3/2$ e^2/h . (D) Horizontal slice at ν_2 showing QH plateaus at 2 , 1 and $3/2$ e^2/h . (E) Table of conductance plateau values as a function of filling factors calculated using Eqs. 1 and 2. Black, purple and red lines correspond to slices in (B), (C) and (D), respectively. (F) Schematic of counter-circulating edge states at filling factors $\nu_1 = -\nu_2 = 2$.

(three from region 1 and one from region 2). All observed conductance plateaus are also seen at $T = 4$ K and for B in the range 4 to 8 T.

We do find some departures between the experimental data and Eqs. 1 and 2, as represented in the grid of Fig. 3E. For instance, the plateau near $3/2$ e^2/h in Fig. 3D is seen at a value of ~ 1.4 e^2/h and no clear plateau at 3 e^2/h is observed for $\nu_1 = -\nu_2 = 6$. We speculate that the conductance in these regions being lower than their expected values is an indication of incomplete mode mixing. We also observe an unexpected peak in conductance at a region in gate voltage between the two 1 e^2/h plateaus at $\nu_1 = \pm\nu_2 = 2$. This rise in conductance is clearly seen for $|V_{TG}|$ values between ~ 1 and 2 V and V_{BG} values between ~ -5 and -2 V. This may result from the possible existence of puddles of electrons and holes near the charge-neutrality points of regions 1 and 2, as previously suggested [26].

We thank L. S. Levitov, D. A. Abanin, C. H. Lewenkopf, and P. Jarillo-Herrero for useful discussions. We thank Z. Chen at IBM T. J. Watson Research Center for suggesting the NO_2 functionalization process and D. Monsma for assistance in implementing it. Research supported in part by INDEX, an NRI Center, and by the Harvard NSEC.

-
- [1] A. K. Geim and K. S. Novoselov, *Nature Mater.* **6**, 183 (2007).
- [2] F. Schedin *et al.*, arXiv:cond-mat/0610809.
- [3] E. H. Hwang *et al.*, arXiv:cond-mat/0610834.
- [4] C. Berger *et al.*, *Science* **312**, 1191 (2006).
- [5] Z. Chen *et al.*, arXiv:cond-mat/0701599.
- [6] M. Y. Han *et al.*, *Phys. Rev. Lett.* **98**, 206805 (2007).
- [7] A. Rycerz, J. Tworzydło and C. W. J. Beenakker, *Nature Phys.* **3**, 172 (2007).
- [8] M. C. Lemme *et al.*, *IEEE Electron Dev. Lett.* **28**, 4 (2007).
- [9] B. Huard *et al.*, *Phys. Rev. Lett.* **98**, 236803 (2007).
- [10] K. S. Novoselov *et al.*, *Science* **306**, 666 (2004).
- [11] K. S. Novoselov *et al.*, *Nature* **438**, 197 (2005).
- [12] Y. Zhang *et al.*, *Nature* **438**, 201 (2005).
- [13] H. B. Heersche *et al.*, *Nature* **446**, 56 (2007).
- [14] M. I. Katsnelson, K. S. Novoselov and A. K. Geim, *Nature Phys.* **2**, 620 (2006).
- [15] V. V. Cheianov and V. I. Fal'ko, *Phys. Rev. B* **74**, 041403(R) (2006).
- [16] V. V. Cheianov, V. I. Fal'ko and B. L. Altshuler, *Science* **315**, 1252 (2007).
- [17] D. R. Smith, J. B. Pendry and M. C. K. Wiltshire, *Science* **305**, 788 (2004).
- [18] D. A. Abanin and L. S. Levitov, *Science* **317**, 641 (2007).
- [19] D. B. Farmer and R. G. Gordon, *Nano Lett.* **6**, 699 (2006).
- [20] V. P. Gusynin and S. G. Sharapov, *Phys. Rev. Lett.* **95**, 146801 (2005).
- [21] D. A. Abanin, P. A. Lee and L. S. Levitov, *Phys. Rev. Lett.* **96**, 176803 (2006).
- [22] N. M. R. Peres, F. Guinea and A. H. Castro Neto, *Phys. Rev. B* **73**, 125411 (2006).
- [23] D. A. Syphers and P. J. Stiles, *Phys. Rev. B* **32**, 6620 (1985).
- [24] R. J. Haug *et al.*, *Phys. Rev. Lett.* **61**, 2797 (1988).
- [25] S. Washburn *et al.*, *Phys. Rev. Lett.* **61**, 2801 (1988).
- [26] E. H. Hwang, S. Adam and S. Das Sarma, *Phys. Rev. Lett.* **98**, 186806 (2007).